

# Uniaxial bond stress-slip behavior of reinforcing bars embedded in lightweight aggregate concrete

Chao-Wei Tang\*

Department of Civil Engineering & Geomatics, Cheng Shiu University, No. 840, Chengcing Rd., Niasong District, Kaohsiung City, Taiwan R.O.C.

(Received September 7, 2016, Revised January 24, 2017, Accepted February 10, 2017)

**Abstract.** This paper presents an experimental study of bond-slip behavior of reinforced lightweight aggregate concrete (LC) and normal weight concrete (NC) with embedded steel bar. Tests were conducted on tension-pull specimens that had cross-sectional dimension with a reinforcing bar embedded in the center section. The experimental variables include concrete strength (20, 40, and 60 MPa) and coarse aggregate type (normal-weight aggregate and reservoir sludge lightweight aggregate). The test results show that as concrete compressive strength increased, the magnitudes of the slip of the LC specimens were greater than those of the NC specimens. Moreover, the bond strength and stiffness approaches zero at the loaded end, or close to the central anchored point of the specimen. In addition, the proposed bond stress-slip equation can effectively estimate the behavior of bond stress and steel bar slipping.

**Keywords:** lightweight aggregate concrete; normal weight concrete; reinforcing bar; bond stress; slip; uniaxial tensile test

## 1. Introduction

Concrete has been described as the essential construction material because of its inherent material properties. However, normal-weight concrete (NC) made with Portland cement and conventional natural aggregate suffers from several defects, such as low tensile strength, less ductile, etc. Fortunately, with the advancement of concrete technology, various attempts to overcome these defects have resulted in the development of special concretes. For instance, lightweight aggregate concrete (LC) is made with lightweight cellular aggregates to replace traditional normal-weight aggregates. Compared with NC, LC possesses many advantages, such as higher strength/weight ratio, lower thermal conductivity, greater durability, and better seismic resistance and fire performance (Somayaji 2001).

The performance of reinforced concrete (RC) structures depends on adequate bond strength between concrete and reinforcing steel (ACI Committee 408 2003). In a RC flexural member, the bending stiffness along the length of the member will vary after cracking. In a cracked RC flexural member, the bending stiffness varies from a minimum value at the location of the crack to a maximum value midway between cracks. Owing to the bond transfer between concrete and reinforcing bars, the intact concrete between adjacent cracks is capable of resisting some tensile stress and thus contributing to the stiffness of the RC member. The contribution of the intact concrete in the

tension zone is often referred to as tension stiffening effect (Zant and Byung 1984).

The stiffness of RC members has a significant effect on load distribution through the structure, and can have a major influence on the cracking and deflection of concrete structures. For accurate assessment of deflection in cracked RC members, tension stiffening effect must be considered in the calculation. International concrete code provisions such as Eurocode 2 (EC2 1993), CEB-FIP model code (CEB 2010) and ACI 318 Code (ACI Committee 318 2014) adopt similar approaches to take in to account the tension stiffening effect. These methods are based on the assumption of perfect bond between concrete and reinforcing bars. However, the bond properties such as bond strength, peak slip and the bond stress-slip relationship of LWC varied greatly from one research to another (Kankam 1997, Husem 2003, Demir and Husem 2015, Mo *et al.* 2015, Shaikh *et al.* 2016). Moreover, different investigators obtain even contradictory results. The significant variations in the bond properties reported by investigators were due to the difference in the bond test methods adopted or type of aggregate used for each investigation (Mo *et al.* 2016).

Numerous studies dealing with mechanical properties have shown that significant differences exist between LC and NC (Husem 2003, Basche *et al.* 2007, Tang *et al.* 2009, Chen *et al.* 2011a, Chen *et al.* 2011b, Tang 2015, Grabois *et al.* 2016). The failure mechanism of LC can differ significantly from NC and depend upon the type of aggregates used and its characteristics. In spite of the increasing use and demand for LC, there is still a lack of adequate explanations to understand the mechanisms responsible for the mechanical properties of LC. In particular, the bond stress-slip relationship in reinforced LC was quite complicated and not yet clearly understood.

\*Corresponding author, Professor  
E-mail: [tangcw@gcloud.csu.edu.tw](mailto:tangcw@gcloud.csu.edu.tw)

Therefore, this study aims to investigate the uniaxial bond stress-slip behavior of reinforcing bars embedded in lightweight aggregate concrete.

## 2. Experimental details

### 2.1 Materials and mix proportions

In this study, the materials used for the preparation of the samples included cement, silica fume, fine and coarse aggregates, superplasticizer, and reinforcing steel. Local ordinary Portland cement (OPC) with a specific gravity of 3.15 and a fineness of 3400 cm<sup>2</sup>/g complying with ASTM C150/C150M (ASTM C150/C150M-15 2015) was used. The silica fume was imported from abroad with a specific gravity of 2.08. Well-graded aggregate and washed natural sand were selected in accordance with ASTM C33/C33M (ASTM C33/C33M-13 2013). The fine aggregate was natural river sand and the normal-weight coarse aggregate was crushed stone with a maximum particle size of 19 mm. Their physical properties are listed in Table 1. The coarse LWA used in this study was locally produced from reservoir sludge. Its physical and mechanical properties are listed in Table 2. Two different superplasticizers (HICON HPC 1000 for medium strength concrete and HICON MTP A40 for high strength concrete) produced by Taiwan Jong Shin Company were used. Their physical properties are shown in Table 3. The reinforcement consisted of one steel reinforcing bar with a 25 mm diameter (No. 8 reinforcing bar). Its physical and mechanical properties are shown in Table 4.

Table 1 Physical properties of normal weight coarse/fine aggregate

Aggregate type	Specific weight (SSD)	Water absorption (SSD) (%)	Unit weight (dry-rodded) (kg/m <sup>3</sup> )	FM
Coarse aggregate	2.63	1.24	1532	-
Fine aggregate	2.56	1.33	-	2.75

Notes: SSD=Saturated surface dry condition; FM=Fineness modulus.

Table 2 Physical and mechanical of LWA

Sieve size	Percent retained (%)	Dry specific weight	Water absorption (%)		Crushing strength (MPa)
			30-min	24-hr	
1/2"-3/8"	64%	1.12	2.82	5.23	7.47
3/8"-4#	36%	1.30	4.12	6.59	

Table 3 Basic properties of superplasticizer

Type	Specific weight	pH value	Solid composition (%)
HPC 1000	1.20	7±1	3.37
MTP A40	1.13	7±1	-

Table 4 Physical and mechanical of deformed bar

Bar No.	Nominal dia. (mm)	Nominal cross section area (cm <sup>2</sup> )	Rib distance (mm)	Rib width (mm)	Rib height (mm)	Elastic modulus (GPa)
8	25.40	5.07	30.4	3.7	1.7	205

Table 5 Mix proportions of LC

Mix No.	W/B	Cement (kg/m <sup>3</sup> )	Silica fume (kg/m <sup>3</sup> )	Water (kg/m <sup>3</sup> )	FA (kg/m <sup>3</sup> )	LWA(kg/m <sup>3</sup> )		SP (kg/m <sup>3</sup> )	Dry unit weight (kg/m <sup>3</sup> )
						1/2"-3/8"	3/8"-4#		
L20	0.78	250	-	195	796	272	178	0	1546
L40	0.48	394	-	189	665	279	182	1.38	1600
L60	0.32	405	45	144	857	240	157	2.48	1740

Note: L=Lightweight aggregate concrete, digits=Strength level, W/B=Water/binder ratio, SP=Superplasticizer (HICON HPC 1000 for L40 and HICON MTP A40 for L60)

Table 6 Mix proportions of NC

Mix No.	Water/cement ratio (W/C)	Cement (kg/m <sup>3</sup> )	Water (kg/m <sup>3</sup> )	Aggregate (kg/m <sup>3</sup> )		SP (kg/m <sup>3</sup> )	Dry unit weight (kg/m <sup>3</sup> )
				FA	CA		
N20	0.76	267	203	772	1054	0	2147
N40	0.52	390	203	670	1054	0.78	2194
N60	0.32	591	189	523	1063	6.50	2301

Note: N=Normal weight aggregate concrete, digits=Strength level, FA=Fine aggregate, CA=Coarse aggregate, SP=Superplasticizer (HICON HPC 1000 for N40 and HICON MTP A40 for N60)

Two different types of concretes, LC and NC, were made. The former is the experimental group, and the latter is the control group. To investigate the influence of concrete strength on the bond behavior, the specified 28-day compressive strengths were chosen equal to 20, 40 and 60 MPa. The mix proportions for the LC and the NC are given in Table 5 and Table 6, respectively. The abbreviations for identifying each concrete indicate the type of concrete - lightweight aggregate concrete (L) or normal-aggregate concrete (N) and the strength of the concrete (20, 40 or 60 MPa).

All the aggregates were treated in a room until the required saturated surface-dry condition was reached. The aggregates were then maintained in a room in which the ambient temperature and relative humidity (RH) were controlled at 25±3°C and 50±5% to prevent moisture changes. In mixing, the cement (silica fume), fine aggregates, and coarse aggregates were fully blended first, and then water and superplasticizer were added. The mixing was continued until a homogeneous concrete without any segregation was obtained.

### 2.2 Casting of specimens

To obtain the actual steel stress during the testing process, the reinforcing bars were cut into two equal parts through the diameter, as shown in Fig. 1. Many researchers

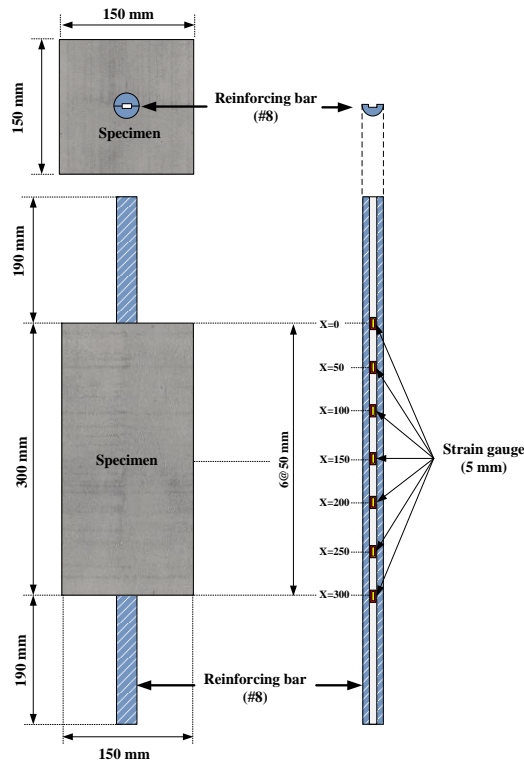


Fig. 1 Dimensions, cross-section, and machined bar of specimen

have adopted this approach (Kankam 1997, Zhao *et al.* 2013). Each swan half-bar was milled to provide a longitudinal groove that was 4 mm wide and 2 mm deep to mount 5 mm long strain gauges with a spacing of 50 mm along the length of the specimen. The upper and lower parts of the reinforcing bars were spot-welded together before being embedded in the concrete specimen. In addition, a thread was prepared at either end of the reinforcing bar to take a nut so as to secure the two halves together.

Fig. 1 shows that the tension-pull specimens had cross-sectional dimension of 150×150 mm and length of 300 mm with a reinforcing bar embedded in the center section. The embedment length in the specimens was 300 mm to represent a crack spacing that was long enough to allow a satisfactory variation of stress in the reinforcing bar and short enough to avoid the formation of a transverse crack in the concrete.

Steel molds were used to cast all the specimens of the uniaxial tensile tests. Freshly mixed concrete was slowly poured into the tension-pull specimen mold and was followed by controlled vibrations to ensure that the concrete was well compacted. Six 100-mm-diameter×200-mm-high cylindrical specimens, referred to hereafter as control cylinders, were also cast with suitable external vibration for each mixture. Following casting, all the specimens were covered overnight with a wet hessian and polyethylene sheets for a period of 24 hours, and then the tension-pull specimens with their respective control cylinders were demolded. After demolding, all specimens were immediately placed in water containers in the laboratory for 27 days. Testing was conducted at 28 days after casting.

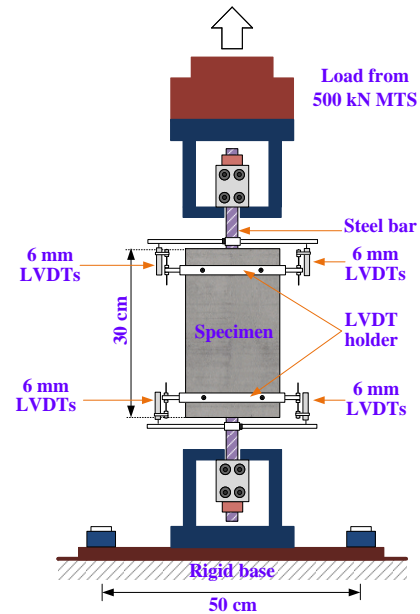


Fig. 2 Setup of uniaxial tensile test

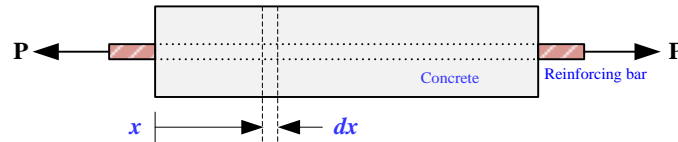
### 2.3 Instrumentation and test procedures

The tension-pull specimens were conducted using a 500 kN MTS servo valve controlled machine equipped with a specially fabricated testing frame as shown in Fig. 2. It can be seen that the relative bond slip between the bar and the concrete was measured by a pair of linear variable differential transformers (LVDTs) on each side of the specimen mounted to the reinforcing bar close to the embedded portion of the specimen. The pullout force was applied under displacement control at a constant rate of 0.01 mm/sec till the design load achieved. Loading was applied monotonically to the specimens in increments of 20 kN from 20 to 160 kN. The pullout force was measured by a load cell fitted in the testing machine. In addition, the test progress was monitored on a computer screen, and each load increment and displacement data were captured and stored in a diskette via a data logger.

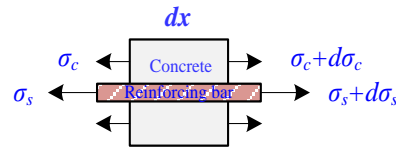
## 3. Analytical model

### 3.1 Definition of the model

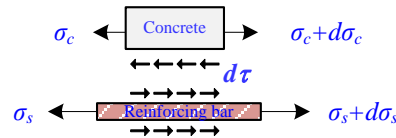
In uniaxial tests, a monotonically increasing tensile force is applied to the two protruding ends of the reinforcing bar embedded in the concrete prism. In this study, the analytical model for analysis of concrete prism is shown in Fig. 3. This model is capable of taking into account the constitutive relationship of constituent materials and introducing the bond-slip relationship at the interface. This characteristic overcomes the hypothesis of no slip between concrete and reinforcing bars. The analytical formulations that dominating the behavior of the element (a single bar embedded in concrete with an infinitesimal length of  $dx$ , as shown in Fig. 3(a)) with reference to the cross section at abscissa  $x$  are summarized as below.



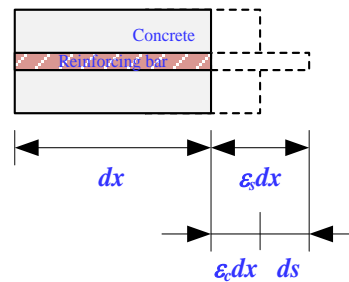
(a) Diagram of tension-pull specimen



(b) Equilibrium of prism



(c) Equilibrium at interface



(d) Consistent deformations

Fig. 3 Analytical model

3.2 Stress and strain of steel

In the tension-pull specimens, the bond stress varies along the embedded length of the reinforcing bar. As mentioned previously, to determine the bond stress along the reinforcing bar, the steel strain is measured using strain gauges attached at various locations (see Fig. 1). Within the elastic ranges of both the concrete and the steel, the linear stress-strain relationships are assumed. In other words, the steel stress was directly proportional to the steel strain within the full range of loading considered in the investigation, as shown below

$$\sigma_s(x) = E_s \varepsilon_s(x) \tag{1}$$

where  $\varepsilon_s$ =steel strain and  $E_s$ =Young's modulus of the steel.

3.3 Stress and strain of concrete

In a generic cross-section of the specimen, from Fig. 3(b), the equation of equilibrium for the prism can be written as

$$P = \sigma_c A_c + \sigma_s A_s \tag{2}$$

where  $P$ =applied normal force;  $\sigma_c$ =stress in the concrete;  $A_c$ =cross-sectional area of the concrete;  $\sigma_s$ =stress in the steel; and  $A_s$ =cross-sectional area of the steel. Further, from Fig. 3(b), the following equilibrium equation must be satisfied

$$d\sigma_c A_c + d\sigma_s A_s = 0 \tag{3}$$

Using Eq. (3), concrete stress in any segment of the prism can be calculated as

$$\sigma_{c,i+1} = \sigma_{c,i} - (A_s/A_c)(\sigma_{s,i+1} - \sigma_{s,i}) \tag{4}$$

Applying the boundary condition (i.e., at  $x=0$ ,  $\sigma_c(0)=0$ ), concrete stress in any segment of the prism can be determined. From the constitutive relationship, the axial strains in the concrete can be calculated as

$$\varepsilon_c(x) = \sigma_c(x) / E_c \tag{5}$$

where  $\varepsilon_c$ =concrete strain and  $E_c$ =Young's modulus of the concrete.

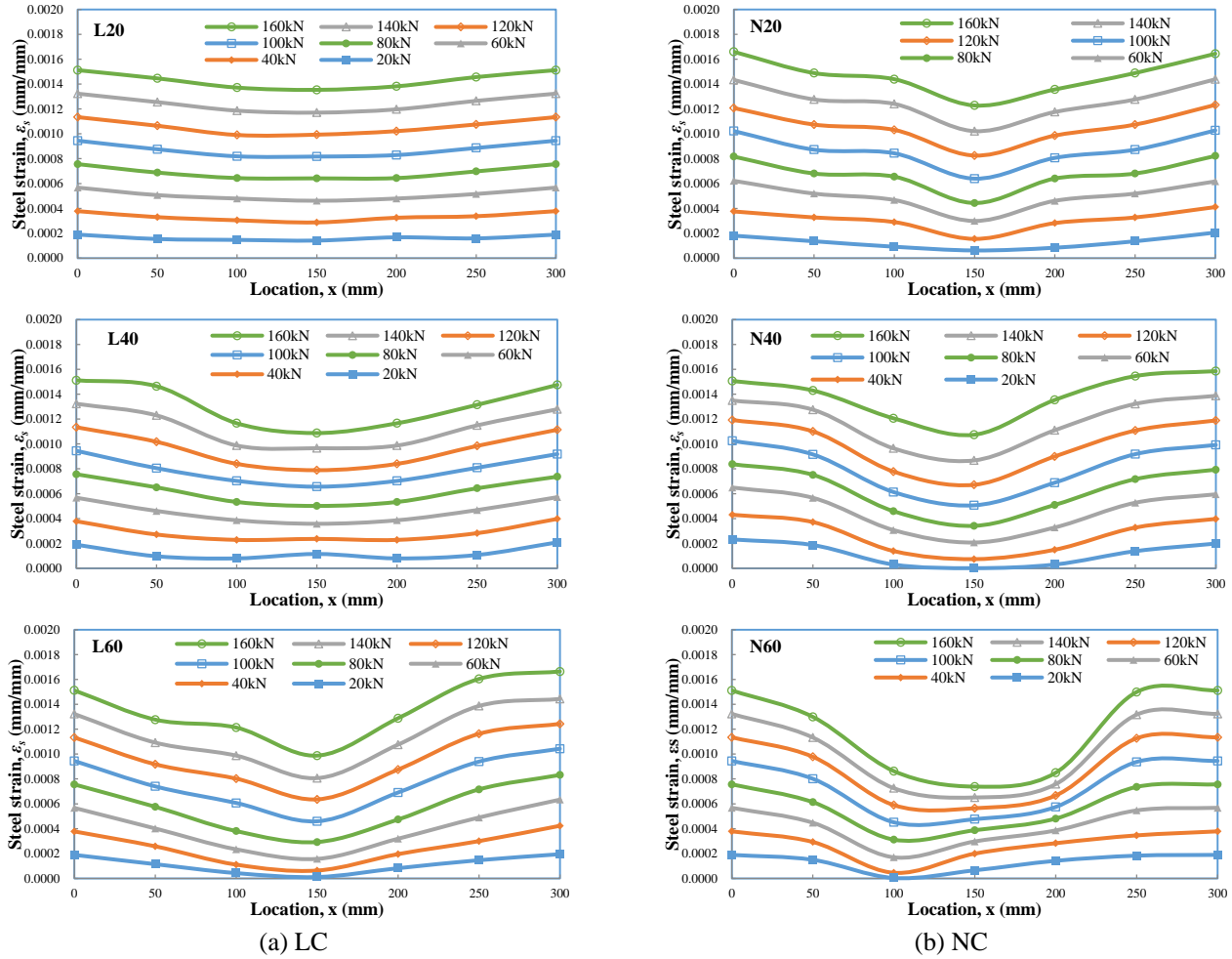


Fig. 4 Strain distribution in reinforcing bars subjected to tensile load

### 3.4 Bond stress

The bond force acting on the reinforcing bar between two strain measurement points is taken as the difference in tensile forces at the two sections. The bond stress is then evaluated by dividing the bond force by the surface area of the reinforcing bar between the two measurement points. From Fig. 3(c), the following equilibrium equation must be satisfied

$$\sigma_{s,i+1} - \sigma_{s,i} = -d\tau \cdot (\pi l_b dx) \quad (6)$$

where  $d\tau$ =relative bond stress between two adjacent positions;  $d_b$ =bar diameter. Applying the boundary condition (i.e., at  $x=0$ ,  $\tau(0)=0$ ), bond stress in any segment of the prism can be calculated as

$$\tau_{i+1} = \tau_i + d\tau \quad (7)$$

### 3.5 Slip between concrete and reinforcing bar

Generally speaking, the bond slips at respective points are determined indirectly using the measured end slip values corresponding to the steel stress at that point. In

addition, based on the consistent deformations as shown in Fig. 3(d), the relative slip at the interface between the concrete and reinforcing bar can be written in the following form

$$ds(x) = -[\varepsilon_s(x) - \varepsilon_c(x)]dx \quad (8)$$

where  $ds(x)$ =relative slip. Applying the boundary condition (at central point of the specimen, slip=0), slip in any segment of the prism can be calculated as

$$s_{i+1} = s_i + ds \quad (9)$$

## 4. Experimental results and discussion

### 4.1 Mechanical properties of concrete

On the day of the uniaxial tensile test, the respective control cylinders were capped and tested in compression to determine the compressive strength of concrete. Mean compressive strength was calculated by taking average of three specimens. Table 7 shows that the average values of 28-day compressive strengths are close to the target values

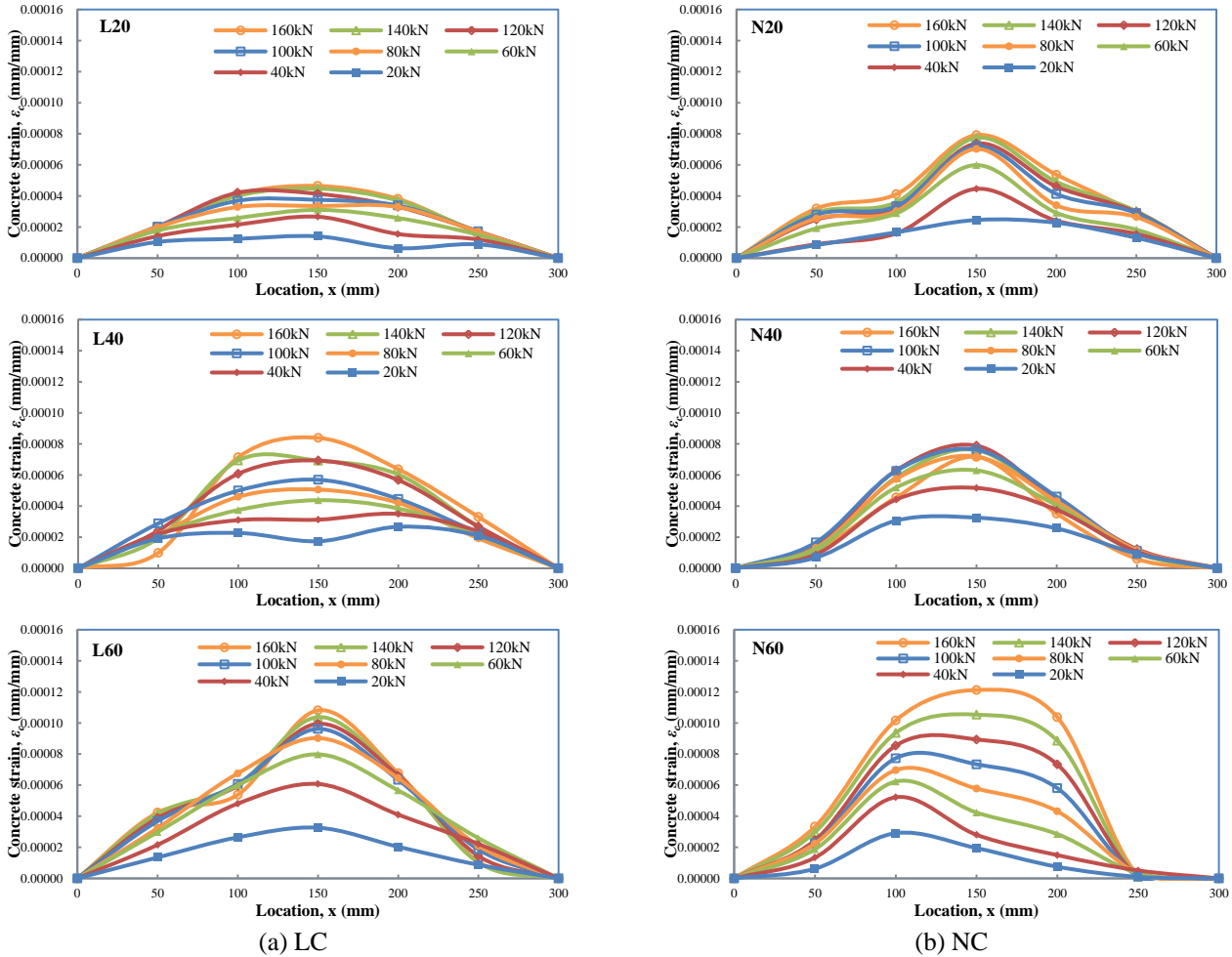


Fig. 5 Strain distribution in concrete subjected to tensile load

Table 7 Mechanical properties of concrete

Mix No.	Compressive strength (MPa)	Splitting strength (MPa)	Elastic modulus (GPa)
N20	20.20	2.40	23.32
N40	40.97	2.91	30.22
N60	59.46	3.23	30.72
L20	20.35	1.65	16.40
L40	40.50	2.03	21.58
L60	58.39	5.15	26.73

(i.e., 20, 40 and 60 MPa). In addition, Table 7 also shows the average values of the splitting tensile strength and elastic modulus of the two types of specimens.

#### 4.2 Steel strain distribution and concrete strain distribution

In tension-pull specimens, the steel strain was measured using strain gauges attached at various locations. Fig. 4 shows curves of the steel strain distribution along the length of reinforcing bars subjected to several increments of static tensile load within the service range. It can be observed that the central regions of the specimen were subjected to

smaller steel strains in comparison with regions near the specimen end. In addition, the steel strain distribution curve for the reinforcing bar showed significant change with an increasing applied load. Overall, for both types of concrete, a typical curve was concave upwards, indicating a minimum steel strain in the center, which is in line with the symmetry of applied load. In other words, the peak point of each steel strain distribution curve occurred at the loaded ends of the bar (i.e., at  $x=0$  mm and  $x=300$  mm) and is symmetric relative to the symmetry axis of specimens.

In addition, Fig. 4 shows little differences in the magnitude of steel strain between the LC and NC specimens under low applied loads. However, as applied load increased, the steel strains near the central regions of the LC specimens were greater than those of the NC specimens. For example, the steel strain at  $x=150$  mm of the L20 specimen was 0.001354 mm/mm, while the steel strain at  $x=150$  mm of the N20 specimen was 0.001238 mm/mm. That is, steel strains decreased with gentle slope towards the midpoint of the LC specimens. This indicates that the tensile concrete stress in the LC specimens was relatively less than that of the tensile concrete stress in the NC specimens under the same axial load. Further, with the increase of concrete compressive strength, the steel strains near the central regions of the LC and NC specimens were

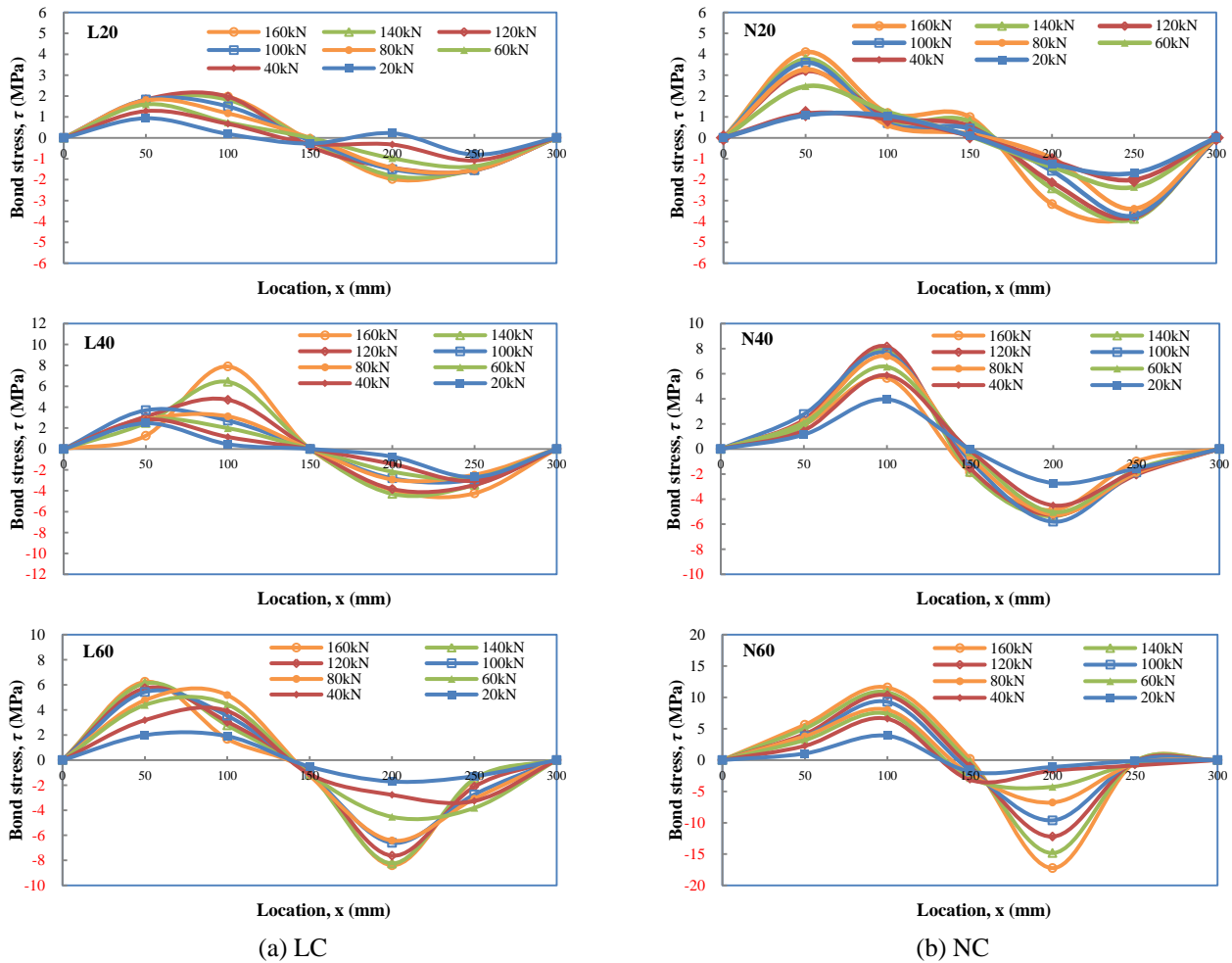


Fig. 6 Distribution of bond stress along reinforcing bars subjected to tensile load

significantly less than those at the loaded ends of the bar. Generally speaking, these large strain differences in the reinforcing bars showed a consistent increase with increasing applied loads.

In the study, the axial stress and the axial strain of concrete were calculated with Eq. (4) and Eq. (5) respectively. Fig. 5 shows that the central regions of the specimen were subjected to larger strains in comparison with regions near the specimen end. Moreover, comparing Fig. 5 with Fig. 4, it can be seen that the concrete strain was less than the steel strain along the overall member length. On the other hand, it can be observed in Fig. 5 that the concrete strains near the central regions of the LC specimens were less than those of the NC specimens. This confirms the results of the foregoing analysis. That is, under the same axial loads, the tensile concrete stress in the LC specimens was relatively less than that in the NC specimens.

#### 4.3 Bond stress distribution and slip distribution

In any segment of the prism specimen, the bond stress developed by the reinforcing bar was calculated with Eq. (7). Fig. 6 shows curves of the bond stress distribution with respect to several increments of static tensile load within the

service range. As can be clearly seen in Fig. 6, as tensile load increasing, there was a consistent increase in the bond stress at almost all points. Further, the maximum value of each curve mainly occurred at, or close to the central anchored point, whereas the minimum value occurred at the anchored midpoint owing to symmetry, or at the loaded end.

The slip between concrete and reinforcing bar was calculated with Eq. (9). Fig. 7 shows curves of the slip distribution of the embedded bars with respect to increasing load within the service range. It can be obviously observed that owing to the symmetry, the magnitude of the slip varied from zero at the anchored midpoint to a maximum at the ends. In addition, as tensile load increasing, there was a consistent increase in the slip at all points except the anchored midpoint. Moreover, with the increase of compressive strength of concrete, the magnitude of the slip distribution curves became smaller. On the other hand, Fig. 7 shows little differences in the magnitude of slip between the LC and NC specimens with low to medium compressive strength. However, as concrete compressive strength increased, the magnitudes of the slip of the LC specimens were greater than those of the NC specimens.

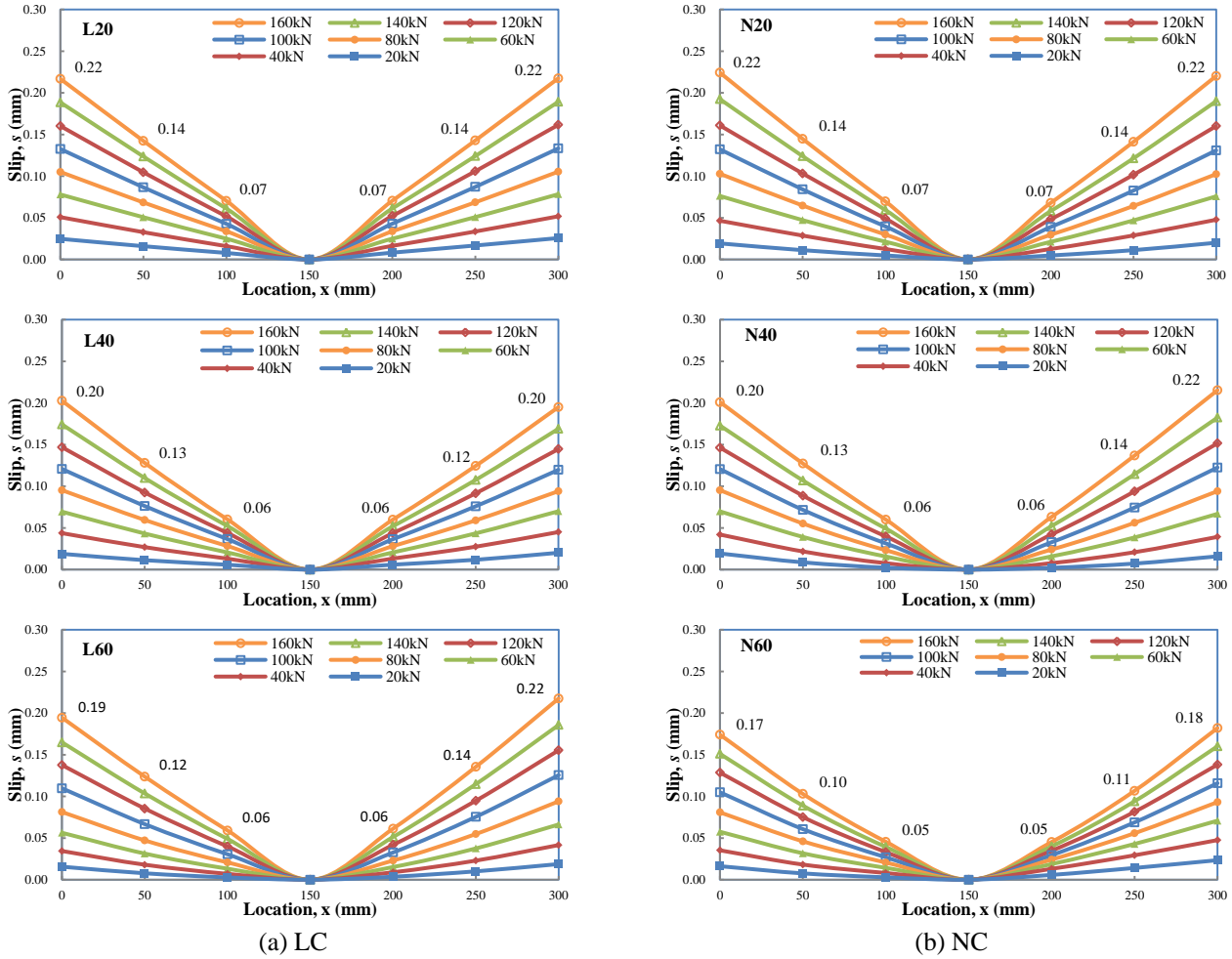


Fig. 7 Distribution of slip along reinforcing bars subjected to tensile load

4.4 Bond stress-slip relationship

According to the previous results of the local bond stress-slip behavior of reinforcing bars embedded in lightweight aggregate concrete (Tang 2015), the local stress and local slip were obtained. Then the ratio of the local stress and local slip is defined as the bond stiffness. The local bond stress at different locations along the bar for a given amount of slip can be connected into a curve. The curve reflects the variation of bond stiffness along the anchoring length. Fig. 8 shows the analytical curves of the relationship between bond stress and slip at different locations along the reinforcing bar for the two types of concrete. As can be easily seen in Fig. 8, the maximum value of each curve mostly occurred at, or close to the central anchored point, whereas the minimum value occurred at the anchored midpoint, or at the loaded end. In other words, the bond strength and stiffness approaches zero at the loaded end, or close to the central anchored point of the specimen. Overall, the maximum value of bond stiffness of the LC specimen about occurred in the vicinity of  $x=0.5l_a$  ( $x$ =distance from the loaded end;  $l_a$ =half the length of the specimen), whereas the maximum value of bond stiffness of the NC specimen about occurred in the vicinity of  $x=0.7l_a$ .

The foregoing analysis showed that the bond stress-slip relationship varies along the reinforcing bar. Besides, it is worth noting that the bond stiffness variation along the specimen reflected the local bond stress-slip relationship at different locations along the reinforcing bar. To describe this change, the local bond stress- relationship can be obtained by the local pullout test (Tang 2015). Then, a distribution function is determined, and the constitutive relationship of the local bond stress and slip is expressed by the product of the two. The shape of distribution function  $\phi(x)$  is used to describe the relative magnitude of bond strength at different locations along the reinforcing bar, as shown in Fig. 9. According to the experimental results of the two types of concretes, the distribution functions and their coefficients of determination obtained by regression analysis can be expressed as follows

$$L20: \phi(x) = 0.47 \left(\frac{x}{l_a}\right)^3 - 3.18 \left(\frac{x}{l_a}\right)^2 + 2.71 \left(\frac{x}{l_a}\right) + 10^{-14} \quad (R^2=0.94) \quad (10)$$

$$L40: \phi(x) = -0.16 \left(\frac{x}{l_a}\right)^3 - 2.08 \left(\frac{x}{l_a}\right)^2 + 2.23 \left(\frac{x}{l_a}\right) - 2 \times 10^{-14} \quad (R^2=0.94) \quad (11)$$

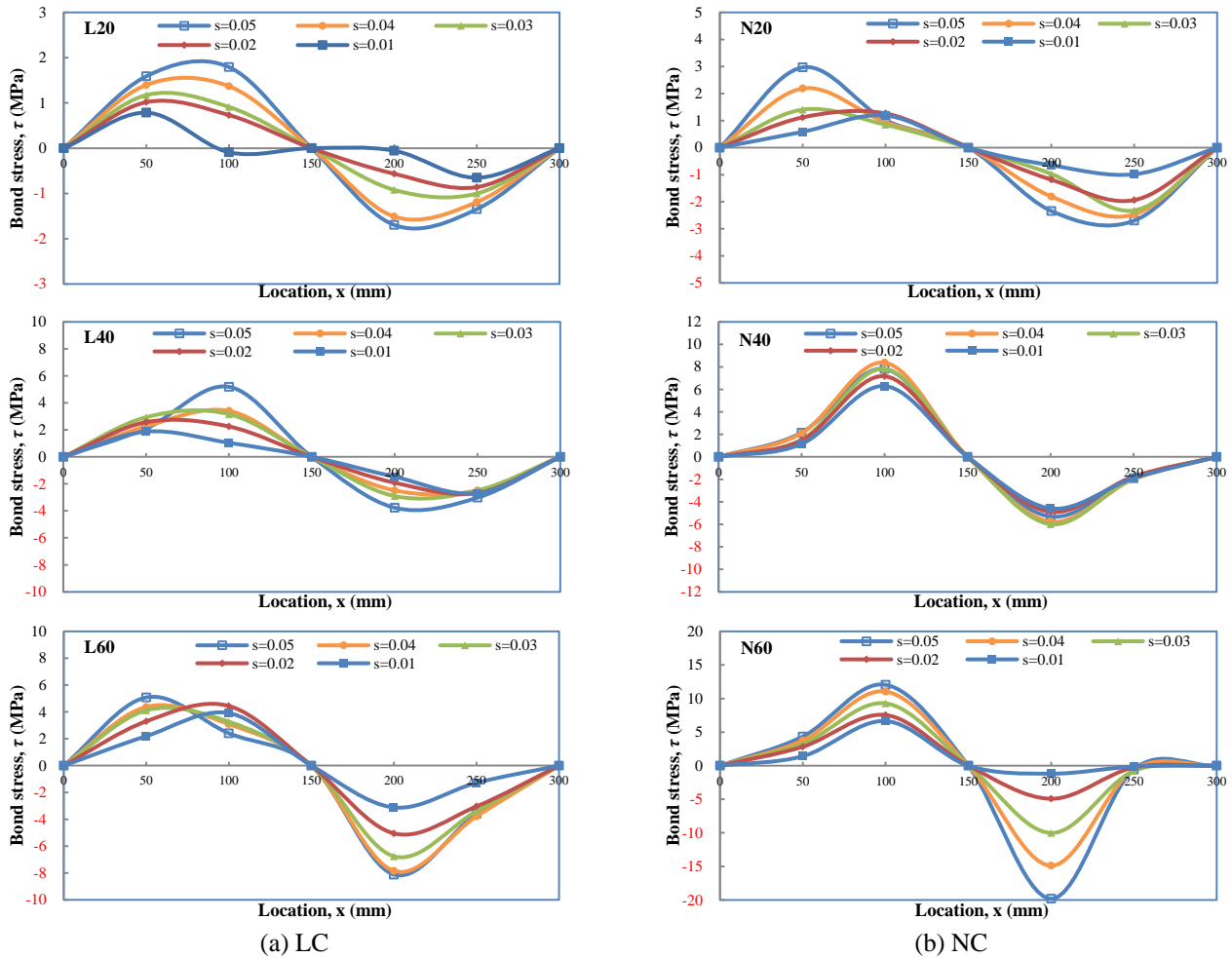


Fig. 8 Bond stress vs. slip relationship

$$\text{L60: } \phi(x) = -1.75 \left(\frac{x}{l_a}\right)^3 + 1.07 \left(\frac{x}{l_a}\right)^2 + 0.68 \left(\frac{x}{l_a}\right) + 10^{-14} \quad (R^2=0.94) \quad (12)$$

$$\text{N20: } \phi(x) = 3.05 \left(\frac{x}{l_a}\right)^3 - 6.72 \left(\frac{x}{l_a}\right)^2 + 3.68 \left(\frac{x}{l_a}\right) - 3 \times 10^{-14} \quad (R^2=0.95) \quad (13)$$

$$\text{N40: } \phi(x) = -10.50 \left(\frac{x}{l_a}\right)^3 - 12.67 \left(\frac{x}{l_a}\right)^2 - 2.16 \left(\frac{x}{l_a}\right) + 2 \times 10^{-14} \quad (R^2=0.95) \quad (14)$$

$$\text{N60: } \phi(x) = -5.93 \left(\frac{x}{l_a}\right)^3 + 6.95 \left(\frac{x}{l_a}\right)^2 - 1.02 \left(\frac{x}{l_a}\right) + 6 \times 10^{-15} \quad (R^2=0.98) \quad (15)$$

In fact, it is able to determine the local bond stress-slip relationship  $\tau(s)$  by the local bond pullout test. Moreover, the distribution function  $\phi(x)$  can be determined as previously stated. Therefore, the bond stress-slip relationship  $\tau(s, x)$  can be expressed as follows

$$\tau(s, x) = \tau(s) \cdot \phi(x) \quad (16)$$

According to the above equation, the bond stress at different locations along the reinforcing bar by the uniaxial tensile test can be calculated for a specific slip. In addition, the analytical results indicate that the proposed bond stress-slip equation can effectively estimate the behavior of bond stress and steel bar slipping.

## 5. Conclusions

The bond stress-slip relationships of reinforcing bars embedded in the LC specimens under uniaxial tensile test were described and compared with companion the NC specimens. Based on the experimental results, the following conclusions can be drawn:

- Under the same axial loads, the tensile concrete stress in the LC specimens was relatively less than that in the NC specimens. Further, with the increase of concrete compressive strength, the steel strains near the central regions of the LC and NC specimens were significantly less than those at the loaded ends of the bar.
- As tensile load increasing, there was a consistent increase in the slip at all points except the anchored midpoint. Moreover, as concrete compressive strength increased, the magnitudes of the slip of the LC

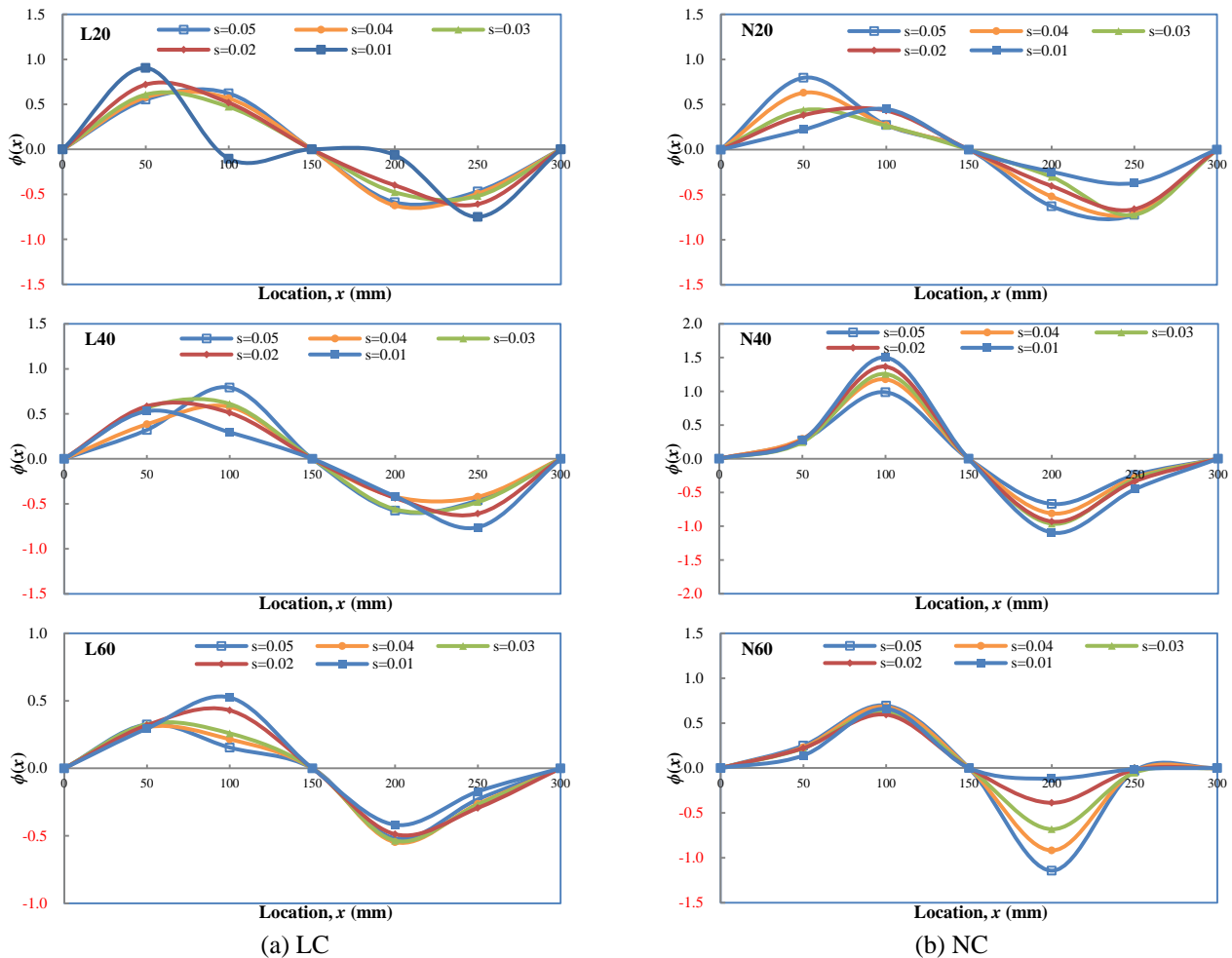


Fig. 9 Distribution function

specimens were greater than those of the NC specimens.

- The bond strength and stiffness approaches zero at the loaded end, or close to the central anchored point of the specimen. The maximum value of bond stiffness for the LC specimen about occurred in the vicinity of  $x=0.5l_a$ , whereas the maximum value of bond stiffness for the NC specimen about occurred in the vicinity of  $x=0.7l_a$ .
- The proposed bond stress-slip constitution relationship can effectively estimate the bond-slip behavior of tension-pull specimens.

## Acknowledgments

The author expresses his gratitude and sincere appreciation to the Ministry of Science and Technology, Taiwan, for financing this research work.

## References

- ACI Committee 224 (1992), Cracking of Concrete Members in Direct Tension (ACI 224.2R-92), American Concrete Institute, Farmington Hills, Mich.
- ACI Committee 318 (2014), Building Code Requirements for Structural Concrete (ACI 318-14) and Commentary, American Concrete Institute, Farmington Hills, Mich.
- ACI Committee 408 (2003), Bond and Development of Straight Reinforcing Bars in Tension (ACI 408R-03). American Concrete Institute, Farmington Hills, Mich.
- ASTM C150/C150M-15 (2015), Standard Specification for Portland Cement, ASTM International, West Conshohocken, PA, www.astm.org.
- ASTM C33/C33M-13 (2013), Standard Specification for Concrete Aggregates, ASTM International, West Conshohocken, PA, www.astm.org.
- Basche, H.D., Rhee, I., Willam, K.J. and Shing, P.B. (2007), "Analysis of shear capacity of lightweight concrete beams", *Eng. Fracture Mech.*, **74**(1-2), 179-193.
- CEB (2010), CEB-FIP Model Code 2010, Lausanne, Switzerland.
- Chen, H.J., Tsai, W.P., Tang, C.W. and Liu, T.H. (2011a), "Time-dependent properties of lightweight concrete using sedimentary lightweight aggregate and its application in prestressed concrete beam", *Struct. Eng. Mech.*, **39**(6), 833-847.
- Chen, H.J., Liu, T.H., Tang, C.W. and Tsai, W.P. (2011b), "Influence of high-cycle fatigue on the tension stiffening behavior of flexural reinforced lightweight aggregate concrete beams", *Struct. Eng. Mech.*, **40**(6), 847-866.
- Demir, S. and Husem, M. (2015), "Investigation of bond-slip modeling methods used in FE analysis of RC members", *Struct. Eng. Mech.*, **56**(2), 275-291.
- EC2 (1993), Eurocode 2: Design of Concrete Structures. ENV 1992-1-2: General Rules - Structural Fire Design. European

- Committee for Standardization, Brussels, Belgium.
- Grabois, T.M., Cordeiro, G.C. and Filho, R.D.T. (2016), "Fresh and hardened-state properties of self-compacting lightweight concrete reinforced with steel fibers", *Constr. Build. Mater.*, **104**, 284-292.
- Husem, M. (2003), "The effects of bond strengths between lightweight and ordinary aggregate-mortar, aggregate-cement paste on the mechanical properties of concrete", *Mater. Sci. Eng. A*, **363**(1), 152-158.
- Kankam, C.K. (1997), "Relationship of bond stress, steel stress and slip in reinforced concrete", *J. Struct. Eng.*, **123**(1), 79-85.
- Mo, K.H., Alengaram, U.J., Visintin, P., Goh, S.H. and Jumaat, M.Z. (2015), "Influence of lightweight aggregate on the bond properties of concrete with various strength grades", *Constr. Build. Mater.*, **84**, 377-386.
- Mo, K.H., Alengaram, U.J. and Jumaat, M.Z. (2016), "Bond properties of lightweight concrete-A review", *Constr. Build. Mater.*, **112**, 478-496.
- Somayaji, S. (2001), *Civil engineering materials*, 3rd ed. New Jersey: Prentice Hall.
- Tang, C.W., Yen, T. and Chen, H.J. (2009), "Shear behavior of reinforced concrete beams made with sedimentary lightweight aggregate without shear reinforcement", *J. Mater. Civ. Eng.*, ASCE, **21**(12), 730-739.
- Tang, C.W. (2015), "Local bond stress-slip behavior of reinforcing bars embedded in lightweight aggregate concrete", *Comput. Concrete*, **16**(3), 449-466.
- Zant, Z.P. and Byung, H.O. (1984), "Deformation of progressively cracking reinforced concrete beams", *ACI J.*, **3**(8), 1268-1278.
- Zhao, Y., Lin, H., Wu, K. and Jin, W. (2013), "Bond behaviour of normal/recycled concrete and corroded steel bars", *Constr. Build. Mater.*, **48**, 348-359.